Evaluation and Benchmarking of Level Set-Based Three Forces via Geometric Active Contours for Segmentation of White Blood Cell Nuclei Shape

Khamael AL-Dulaimi[a,*], Inmaculada Tomeo-Reyes[b], Jasmine Banks[a], Vinod Chandran[a]

[a]*School of Electrical Engineering and Computer Science, Queensland University of Technology, QLD, Australia*
[b]*School of Electrical Engineering and Telecommunications,University of New South Wales, NSW, Australia*

Abstract

The segmentation of white blood cells and their nuclei is still difficult and challenging for many reasons, including the differences in their colour, shape, background and staining techniques, the overlapping of cells, and changing cell topologies. This paper shows how these challenges can be addressed by using level set forces via edge-based geometric active contours. In this work, three level set forces (curvature-based, normal direction, and vector field-based) are comprehensively studied in the context of the problem of segmenting white blood cell nuclei based on geometric flows. Cell images are first pre-processed, using contrast stretching and morphological opening and closing in order to standardise the image colour intensity, to create an initial estimate of the cell foreground and to remove the narrow links between lobes and cell bulges. Next, segmentation is conducted to prune out the white blood cell nucleus region from the cell wall and cytoplasm by combining the theory of curve evolution using curvature-based, normal direction, and vector field-based level set forces and edge-based geometric active contours. We show that the proposed method allows the front interface to propagate naturally despite significant protrusions, topological changes and narrow regions. The results are stable, and provide smooth cell boundaries to discriminate the white blood cell nuclei. The overall performance of the proposed segmentation method is compared and benchmarked against existing techniques for nucleus shape detection, using the same databases. The three level set forces studied here (curvature, normal direction, and vector field) via edge-based geometric active contours achieve F-index values of 92.09%, 91.13%, and 90.76%, respectively, and the proposed segmentation method results in better performance than all other techniques for all indices, including Jaccard distance, boundary displacement error, and rand index.

Keywords: `White blood cell nuclei, microscope images, segmentation, level set-based three forces, edge-based geometric active contours, evaluation, benchmarking.`

*Corresponding author
Email addresses: `khamaelabbaskhudhair.aldulaimi@hdr.qut.edu.au` (Khamael AL-Dulaimi), `i.tomeo-reyes@unsw.edu.au` (Inmaculada Tomeo-Reyes), `j.banks@qut.edu.au` (Jasmine Banks), `v.chandran@qut.edu.au` (Vinod Chandran)

1. Introduction

White blood cells (WBCs) are an important part of the human immune system and play a key role in fighting infections. The automated identification and counting of WBCs can aid in the diagnosis of different diseases, such as leukaemia and other types of cancer, and certain immunological disorders [1]. In clinical diagnosis, WBCs are analysed using peripheral blood smear and bone marrow samples from patients. Samples are prepared for microscope imaging using a slide and a staining process, resulting in different colourations of the WBC nuclei, cytoplasm, plasma, and red blood cells (RBCs). There are many types of stain, such as the Giemsa, Wright, Wright-Giemsa, and Leishman stains, and most of these dye the nucleus dark purple or pink. The slides are placed under a compound or optical microscope at certain light intensities and magnifications, and a digital camera is used to obtain images [2, 3]. These digital images can be manually (visually) examined or processed using digital image processing techniques and machine learning algorithms to generate automated reports. The steps in the manual segmentation process include the collection of blood; preparation of the blood smear, viewing using a microscope, the expert's decision, and the final report. If a decision can not be made, a new blood smear is prepared and the steps repeated. This traditional procedure of examining WBCs needs a haematologist to manually count and segment the cells with the help of a microscope. The manual segmenting of WBCs involves several difficulties, since:(a) it is time consuming; (b) it involves a large amount of work for experts in relation to the output result; (c) more than two experts are required to make a decision on the detection of WBCs; and (d) it is difficult to distinguish between WBCs and other components of blood cells, including red blood cells (RBCs), plasma, cytoplasm and background. Experts can identify the different types of WBCs in the body based on the way their nuclei appear. The shapes of WBC nuclei provide information about the type of illness or infection; for example, inflammation and blood diseases can cause an increase or decrease in the number of certain types of WBCs in the human body, or may change the shape and size of WBC nuclei. Segmentation is not complex for trained professionals such as pathologists, who use the geometrical, textural, and morphological information of the WBC nuclei to segment and differentiate them, and to determine which cells are normal or abnormal. However, the complex natures of the pathologies and the microscopy images presents significant challenges for the manual analysis of images, which can lead to large inter-observer variations. In addition, the manual segmentation of WBC nuclei is a time-consuming, repetitive task. Pathologists therefore need an automated segmentation system that can provide fast reproducible image analysis so that science researchers and clinician scientists can be released from boring and repeated routine efforts. In this paper, we aim to design a framework with the ability to segment WBC nuclei, and investigate the classification of WBCs into three types and seven sub-types. Based on this,

the results of segmentation are fed into a feature calculation and representation stage, which then feeds into a classification stage. Segmentation of the nucleus provides rich features which are found to be sufficient for classification, and it is not necessary to use features of the cytoplasm for classification. The automated processing of WBC images involves the pre-processing, segmentation and classification of WBCs into types and sub-types; there are three types and seven sub-types of WBCs, as shown in Fig-1. Further details of the characteristics of WBC nuclei, including their shape, texture, size and number of lobes, can be found in [4].

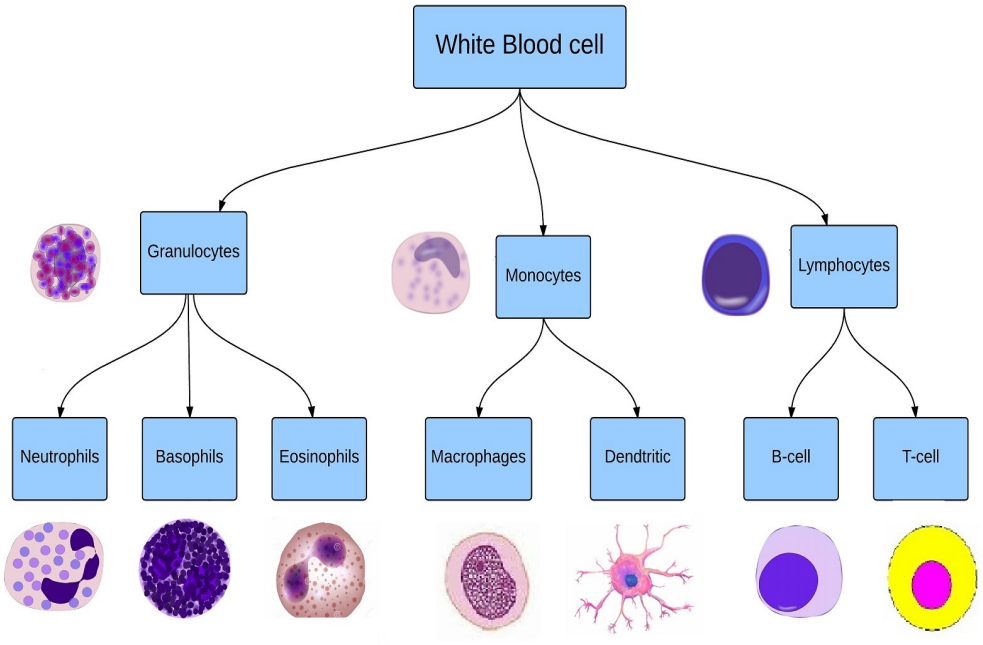

Figure 1: WBC taxonomy from bone marrow [4].

1.1. Motivation and Contributions

The detection of cell nuclei is very important in the task of WBC classification and in the diagnosis of disease. Information about the shape of the nucleus is sufficient to predict the WBC type and sub-type and to diagnose disease. Many techniques have been used to segment WBCs, and their nuclei and have obtained high accuracy. The advantages of these methods in helping to detect the whole WBC is that they use different background colour, dyeing conditions, and capture at different illumination levels that cause different colour spaces in images, as in [5, 6, 7, 8, 9, 10]. They have also been used to reduce the computational complexity, as in [11, 12]. The results of segmentation of WBCs and their nuclei have been used to localise some WBC types, including monocytes, lymphocytes, basophils, neutrophils, and eosinophils, in [13, 14, 15]. However, this type of segmentation is still challenging, for many reasons. Firstly, microscope images of WBCs involve a wide range of shapes, textures, positions and colouring

and this affects reliable segmentation. According to the literature, it is difficult to reliably discriminate between the nucleus and the cytoplasm, since the different types of illumination used in microscope image acquisition may lead to different colour distributions for the nucleus and cytoplasm regions. Secondly, cells have different sizes, shapes and levels of cell-cytoplasm contrast during different phases of maturation, making it difficult, even for pathologists, to identify cells and distinguish the nucleus from the cytoplasm and adjacent erythrocytes. Thirdly, the variation in the complex cell and nucleus boundaries, the overlapping of cells, the presence of deformed cells and the use of different staining techniques make it difficult to track changes in cell boundary topology. Difficulties can arise when cells are merging or splitting, or when boundaries are concave, convex, or have sharp corners. Most of the existing techniques were proposed to segment and detect whole WBCs (i.e. the nucleus and cytoplasm together). This can introduce difficulties since some cells do not have a nucleus, and others have a large nucleus that covers the whole cell. Some methods rely on the colour of WBCs to distinguish between the cell and its nucleus, and this also introduces difficulties due to the use of different types of staining during the preparation of WBC slides.

The main contribution of this paper is the presentation for the first time of a general framework for modelling the evolution of curve boundaries and geometric flows for WBC nuclei segmentation using a combination of level set forces (normal direction and vector field) and edge-based geometric active contours (GACs) to address the nucleus segmentation problem.

- Normal direction-based level set forces with edge-based GACs are used to address the nucleus segmentation problem in the context of merging, splitting, and concavity, of the lobes of nuclei.

- Vector field-based level set forces with edge-based GACs are used to address the nucleus segmentation problem in the context of sharp corners and irregular shapes.

Curvature-based level set forces with edge-based GACs, which were used in [16, 17] and in prior work [18] to obtain shape information to classify WBCs, can also be used to address the nucleus segmentation problem in the context of regular shape and curve propagation. The performance of all three level set forces is critically evaluated here. We focus on the combination of level set forces with GACs and their effects on topological changes, such as merging, splitting, concavity, convexity, sharp corners and curve propagation, in the context of the WBC nucleus segmentation problem. The segmentation performance is evaluated and benchmarked using the F-index and other matrices, and the three forces are compared against other techniques. To the best of our knowledge, the proposed methodology has not previously been applied to the segmentation of WBC nuclei in microscope images in the manner used in this work. The results of our study can potentially be applied to the WBC classification and counting framework to speed up the diagnosis of disease.

1.2. Literature Review

Image segmentation is the process of dividing an image into multiple parts corresponding to different objects or parts of objects. Image segmentation can be used in numerous fields, such as object detection [19, 20], biometric detection [21, 22], speaker recognition [23], facial recognition [24, 25], steganography [26, 27, 28], satellite imaging [29], and medical imaging [30, 31]. One major difficulty with medical image segmentation is the high variability in medical images due to the different modalities used to create medical images, such as X-ray [32], ultrasound [33], CT [34], MRI [35], microscopy [36], PET [37], SPECT [38], endoscopy, OCT [39], and many more. The results of segmentation can then be used to obtain further diagnostic insights. Recent applications have used several techniques, such as graph-based segmentation [40], segmentation-based deep neural networks [41], and segmentation based faster R-CNN and U-net networks [42].

Some methods have been used for decades to detect and segment WBC images (nucleus and cytoplasm together). These include thresholding techniques [43], morphological operators and scale-space analysis [44], edge and boundary detection [5], multiscale analysis [6], colour space-based k-means clustering [7], fuzzy c-means (FCM) [8], dual thresholding [9] and Otsu's thresholding [10]. More recent techniques include colour spaces with Otsu's threshold [45], the k-means clustering method, the Gram-Schmidt orthogonal process [11], k-means clustering with a modified watershed algorithm [46], and optimal thresholding and manifold-based low-rank representation (HTLRR) [12]. A segmentation method was proposed in [13] to detect WBCs using a colour band and thresholding procedure, combining colour spaces with Otsu's thresholding and morphological filters. Deep learning (DL) techniques have been also used to segment WBCs, such as a self-supervised learning method in [14] and a marker-controlled watershed-based neural network algorithm in [15].

However, these methods rely on the colour of WBCs, thresholding techniques or clustering techniques or edge detection to distinguish between the cell and its nucleus, and these processes introduce new difficulties due to the use of different staining methods during the preparation of WBC slides, and the different shapes, levels illumination and stages of maturity involved. WBC nuclei contain the most useful information required for the segmentation, feature extraction and classification of cells, meaning that the accurate segmentation of WBC nuclei is essential. Recent research into DL in the field of computer vision and image processing has opened up possibilities for combining this approach it with different techniques and applying it to different fields. DL methods, and especially artificial neural networks (ANNs) [15], have been applied in the segmentation of WBCs. Currently, DL approaches to this problem are still in the early stages of exploration and investigation, and are outside the scope of our work.

Despite previous work in this field, the automatic segmentation of WBCs based on nuclei shape is still challenging, particularly in the presence of non-uniform illumination, overlapped cells, different shaped

of nuclei, and cell distortion. The level set method using curvature, normal direction and vector field forces with edge-based GACs can be used to address the WBC nucleus shape segmentation problem because of the ability of level set methods to perform well in the presence of concavities, convexities and propagating curves, and the ability of active contours to follow geometric shape.

1.2.1. Level Set Method and Active Contours

The level set method was proposed by Osher *et al.* [47, 48] to solve the problems of concavities, convexities and propagating curves, and has since been used in image processing, computer vision, fluid mechanics and several other fields. Many techniques have been used in conjunction with level set methods to detect the boundary of an object, such as snake and region-based methods, and a watershed algorithm [48].

There are two types of active contours: parametric active contours (PACs) and geometric active contours (GACs).

PACs, also known as snakes, have been extensively used in computer vision and computer graphics for the segmentation, visualisation, detection, and quantification of different anatomic structures [49]. PACs represent curves and surfaces explicitly in their parametric forms during deformation, as parameterised boundaries in a Lagrangian formulation. This representation allows issues of shape estimation to be solved by reducing energy functions that potentially evolve to a minimum value when contours are smooth and reside at the boundaries of an object. However, the method has limitations when there are deformations in the object boundaries. For example, splitting or merging parts of an object can be difficult using a parametric capture range. PACs also have a concavity convergence problem [50].

GACs were proposed by Caselles *et al.* [51] to solve the problem of changes in curve topology by using curve evolution, and have been used in image processing for the edge detection and segmentation of different types of medical images. GACs represent curves and surfaces implicitly, as level sets of a 2D distance function evolving according to an Eulerian formulation. They are based on level set techniques implemented via the theory of curve evolution, and do not use control points to determine the boundaries. GACs may be edge-based or region-based; edge-based GACs use an image gradient to construct an edge stopping function to stop the contour evolution at the object boundaries while region-based GACs use statistical information inside and outside the contour to control the evolution and to calculate the energy based on the mean value of the intensity. Edge-based segmentation algorithms give better precision on the edges along the object boundary, whereas region-based segmentation algorithms perform better with images that have homogeneous intensity in each of the regions to be segmented.

The advantage of the level set method via GACs is that it can perform numerical computations involving curves, shapes and surfaces based on a fixed Cartesian grid, without having to reparameterise them. It can rapidly detect the edges of an object and handle topological changes naturally since

parameterisation take place after deformation is completed [52].

1.2.2. Application of Level Set Method and Active Contours

Many techniques have been used in the segmentation of histological images, including some that have been developed using GACs. In [53], a watershed technique based on GACs was applied to segment histological images. Three different metaheuristics (real-coded GA, particle swarm optimisation and differential evolution) and two classical segmentation algorithms (the Chan and Vese model and GACs) were used in [54]. An active contour model (ACM) implemented using the level set method of segmenting vessels from TOF-MRA data was used in [55]. A self-adaptive weighted level set evolution method was used in [56] for the segmentation of parotid ducts. However, the limitations of these techniques are: (i) their inability to resolve the boundaries of intersecting objects; and (ii) their lack of robustness to occlusion. Multiple overlapping objects are typically segmented as a single object. Although the level set method has been extensively used in cell detection, few research works use it for WBC segmentation. A technique using the level set method via threshold decomposition was proposed in [57] for the tracking and detection of WBC boundaries based on shape and intensity features. This algorithm failed to segment or detect cell nuclei, and was computationally intensive. In [58], a region detection model and expectation-maximisation (EM) algorithm were used to obtain intensity features, which helped in estimating an initial contour evolved using the level set method. The algorithm failed to detect cells when the shapes of the WBCs were excessively deformed, and also failed to discriminate between erythrocytes and WBCs when regions of touching erythrocytes with high density appeared similar to WBCs. It also could not distinguish between the nucleus and the cytoplasm, if the cytoplasm granules had the same darkness as the nucleus or if they had the same brightness as the background. A modified level set method was used in [59] to detect and distinguish cancer cells from WBCs. However, while this algorithm detected and located large cells, small and overlapped cells were not detected. Level set-based active contours were proposed in [60] to detect Hep-2 cells, and this study explored overlapped cells (multiple cells). In [18], a level set method-based curvature force via GACs was proposed to segment WBC nuclei, and the segmentation performance was compared with several other methods using the Berkeley database. WBC nucleus segmentation was addressed in [18] using curvature-based forces via GACs. To date, the level set method via edge-based GACs using forces in the normal direction and vector field-based forces has not been used for WBC nuclei segmentation. In 2017, the level set method was developed using DL, and was applied to medical image analysis in [61]. However, the use of the level set method adapted with DL techniques in the medical image segmentation is still limited and challenging, since medical images are complex and diverse. The use of the level set method and active contours adapted with DL techniques in segmentation of WBCs should therefore be investigated in the future.

The rest of the paper is organised as follows: The proposed method is explained in Section-2. The experimental results and a discussion are presented in Section-3. Finally, Section-4 gives the conclusions of the study.

2. Proposed Method

In this paper, a new framework is proposed for segmenting WBC nuclei using GACs with level set forces. The level set method is used to calculate an implicit surface based on curvature-based forces, forces in the normal direction, and vector field-based forces, while GACs are used to track the interface and the shape of WBC nuclei.

In the level set method, an initial curve known as a zero level set evolves to the boundaries of objects based on the image pixels $I(x, y)$. The zero level set is where the level set function has the value zero, and this is considered the initial contour. The zero level set C can be written as [48]:

$$C = \{(x, y)|\phi(x, y) = 0\} \tag{1}$$

A signed distance function is used to represent the interface C implicitly. The level set function is initialised as the signed distance from the pixel position (x, y) to the interface C:

$$\phi(x, y) = \pm d((x, y), C) \tag{2}$$

This distance is positive if the pixel is inside C, negative if the pixel is outside C, and zero if the pixel is on C. In this study, the signed distance is used only once for initialisation of the level set function, and is not used again (see Algorithm-1 in Section 3.2.1).

The evolution of the surface over time is controlled by forces. The force F, also known as speed, may be a curvature-based force, a force in the normal direction, or a vector field-based force. The force F at a point on the surface normal to the surface is used to pull or push the contour according to the following equation [48]:

$$\frac{\partial\phi(x, y, t)}{\partial t} + F\,|\nabla\phi(x, y, t)| = 0 \tag{3}$$

Forward Euler discretisation is used for temporal discretisation. As a result, the level set equation can be written as [48]:

$$\frac{\phi^{n+1} - \phi^n}{\Delta t} + F^n\,|\nabla\phi^n| = 0 \tag{4}$$

which can be further expanded to [47]:

$$\frac{\phi^{n+1} - \phi^n}{\Delta t} + u^n\phi_x^n + v^n\phi_y^n = 0 \tag{5}$$

where ϕ^{n+1} is the value of ϕ at time $n+1$, ϕ^n is the value of ϕ at time n, and Δt is the Euler time step, which can be calculated as follows:

$$\Delta t \; max \left\{ \frac{|u|}{\Delta x} + \frac{|v|}{\Delta y} \right\} = \beta \tag{6}$$

where $0 < \beta < 1$.

Spatial discretisation is used to calculate $|\nabla\phi|$. It is based on 3^{rd} order Hamilton-Jacobi essentially non-oscillatory schemes (HJ ENO), as explained in detail in [48]. The basic idea of ENO schemes is the use of a higher order accurate polynomial to reconstruct ϕ and then differentiate it to obtain approximations of ϕ_x and ϕ_y, which are the first-order partial derivatives of $\phi(x, y, t)$ with respect to x and y, respectively.

2.1. Developing Level Set-Based Curvature Force via GACs

In this case, the force F is based on the curvature κ of the curve. Here, the motion is proportional to the curvature and depends on the diffusion equation but with a curve embedded in 2D. The level set equation is written as:

$$\frac{\partial\phi(x, y, t)}{\partial t} + \alpha\kappa \left|\nabla\phi(x, y, t)\right| = 0 \tag{7}$$

where κ is the mean curvature and α is a constant used to weight the curvature-based force. Since the curvature can be either positive or negative (depending on whether the curve is turning clockwise or counter-clockwise), some parts of the curve move outwards while others move inwards. Parameter α balances the regularity of the curve. For $\alpha > 0$, the interface moves in the normal direction, the curve becomes smooth, and shrinks while $\alpha < 0$, the interface moves opposite to the normal direction, and the curve is irregular. When $\alpha = 0$ this equation reduces to the trivial $\phi t = 0$, where ϕ is a constant for all time.

The curvature κ is defined as follows:

$$\kappa = \nabla \cdot \frac{\nabla\phi}{\|\nabla\phi\|} \tag{8}$$

and can be calculated based on Hamilton-Jacobi equations using the ENO3 scheme [47]:

$$\kappa = \frac{\phi_{xx}\phi_y^2 - 2\phi_x\phi_y\phi_{xy} + \phi_{yy}\phi_x^2}{\left(\phi_x^2 + \phi_y^2\right)^{3/2}} \tag{9}$$

where ϕ_x and ϕ_y denote the first-order partial derivatives of $\phi(x, y, t)$ with respect to x and y, respectively; and ϕ_{xx}, ϕ_{yy} and ϕ_{xy} denote the second-order partial derivatives of $\phi(x, y, t)$ with respect to the indicated variables.

The level set method is combined here with edge-based GACs to segment WBC nuclei, using the following evolution equation [62, 63]:

$$\frac{\partial \phi(x,y,t)}{\partial t} = g(I(x,y))(\alpha\kappa + V_0)|\nabla\phi(x,y,t)| \tag{10}$$

Two energies are used in the level set method via edge-based GACs: the level set curvature-based force (internal energy) maintains a smooth contour at the time of deformation, and the terms V_0 and g (external forces) regularise the contour towards the nucleus boundaries. More specifically, V_0 is a constant value that keeps the evolution moving in the proper direction, so that the value of $(\alpha\kappa + V_0)$ is always positive. This constant behaves as a force pushing the curve towards the cell boundary when the curvature becomes negative, i.e. choosing a positive value of V_0 increases the propagation speed and makes the curve shrink, whereas choosing a negative value of V_0 makes the curve expand. The value of α is between 0 and 1, and controls the balance between the robustness and regularity of the contour evolution. The term $g(I(x,y))$ is the edge stopping function, which is a positive and decreasing function calculated from the gradient of an image $I(x,y)$ as follows:

$$g(I(x,y)) = \frac{1}{|1 + \nabla I(x,y)|} \tag{11}$$

The stopping function is used to stop the contour evolution at the cell boundaries. This solves the issues of the level set method related to splitting, merging and concavities, as it preserves the geometric properties of the curve and has the ability to stop the contour when matching the cell boundaries during topological changes.

2.2. Developing Level Set-Based Normal Direction Force via GACs

In this case, the force F is a force in the normal direction of the curve. The level set equation is written as:

$$\frac{\partial \phi(x,y,t)}{\partial t} + V_n\,|\nabla\phi(x,y,t)| = 0 \tag{12}$$

where V_n is the force in the normal direction and $V_n\,|\nabla\phi(x,y,t)|$ represents the amount of evolution under this force. Here, GACs are applied based on the formula below:

$$\frac{\partial \phi(x,y,t)}{\partial t} = g(I(x,y))(V_n + V_0)\,|\nabla\phi(x,y,t)| \tag{13}$$

where $(V_n + V_0)$ determines the overall evolution speed of the level sets along their normal direction, and V_0 is a constant value [51]. The function $g(I(x,y))$ is the stopping function has previously mentioned and defined in in Equation-11.

2.3. Developing Level Set-Based Vector Field Force via GACs

In the level set method based on vector field-based forces, the force F is an external vector field $\overrightarrow{S}$ that pulls the curve towards the edges and sharpens the image around them [48]. The level set equation is written as follows in this case:

$$\frac{\partial \phi(x,y,t)}{\partial t} + \overrightarrow{S}\,|\nabla \phi(x,y,t)| = 0 \tag{14}$$

Forward Euler discretisation is used for temporal discretisation. Spatial discretisation used to calculate $|\,(\nabla \phi(x,y,t))|$ is based on 3rd order ENO and an upwind differencing scheme. The basic idea of an upwind differencing scheme is that the spatial discretisation is chosen based on the direction of the diffusion of information. The level set equation after discretisation is Equation-5, where Δt is calculated using the Euler time step in Equation-6. In Equation-6, $|u|$ and $|v|$ are, respectively, the x and y components of the vector field, which can be calculated as follows:

$$u = c\frac{-x}{\sqrt{x^2+y^2}}\ , v = c\frac{-y}{\sqrt{x^2+y^2}} \tag{15}$$

where c is constant value. When choosing a positive value of c, the curve expands while choosing a negative value of c, the curve shrinks or splits.

GACs are also applied to the level set method using vector field-based forces according to the following equation:

$$\frac{\partial \phi(x,y,t)}{\partial t} = g(I(x,y))(\overrightarrow{S} + V_0)\,|\nabla \phi(x,y,t)| \tag{16}$$

where $(\overrightarrow{S} + V_0)$ determines the overall evolution speed of the level sets along the vector field, and V_0 is a constant value [51]. The function $g(I(x,y))$ is the stopping function, defined in Equation-(11).

Equation-13 is developed from Equation-12 which represents a force (F) in the normal direction to the evaluation curve (as explained in Equation-3 which is a definition of the level set method taken from [48]. The level set method (Equation-3)) is used to calculate an implicit surface based on three forces (F): curvature-based forces Equation-7, forces in the normal direction Equation-12, and vector field-based forces Equation-14. In Equation-12, V_n is the force in the normal direction representing the amount of evolution under this force (external force) in direction of the curve. We developed the Equation-12 by combining the GACS which term $g(f(I,j))$. The term $g(I(x;y))$ in Equation-11 is the edge stopping function, which is a positive and decreasing function calculated from the gradient of an image $I(x;y)$ that helps the external force to follow the geometric shape. V_0 is the force that pushes the curve in the normal direction V_n of the contour, until it converges to the boundary of the gradient g of the image and weak edges disappear.

3. Experimental Results

3.1. Databases

Three public databases are used in this study to evaluate the proposed segmentation framework as follows:

- *Cellavision Database* [64]:
  This database was downloaded from the cellavision competency software databases. It contains $1-140$ slides, which were stained using the May-G̈runwald-Giemsa or Wright staining protocols. Each slide contains approximately 103–112 WBCs and a large number of RBCs. Images were taken from both peripheral blood and body fluid blood, with resolution 157×157 pixels. In this database, images are divided into single cells and multiple cells, and each of these groups is divided into normal and abnormal cells. All of the normal single cells were used for the work in this paper, comprising a total of 350 images.

- *Acute Lymphoblastic Leukemia Image Database for Image Processing* (*ALL-IDB*) [65]:
  This database was collected by the Department of Information Technology - Università degli Studi di Milano. It contains 250 microscope single-cell images of size 2592×1944 pixels.

- *Wadsworth Centre* [66]:
  This database contains 150 single cell images at magnification ranges of between 500 and 1000. The contrast between the cell and the background depends on the thickness and lightness of the smear, the illumination, and the staining process used to stain the nucleus (Giemsa, Wright or Wright-Giemsa staining). The image size is 150×150 pixels.

3.2. Proposed Approach Implementation

The proposed segmentation framework is tested using 750 digital images of different types of WBCs: 350 single cell images from the Cellavision database, 250 single cell images from ALL-IDB, and 150 single cell images from the Wadsworth Centre database. The proposed method is implemented using 24 BMP images. The ground truth for all images is obtained manually using MATLAB 2016a, and a MATLAB code is created to track the cell shape using a pointer, with the help of two pathologists. The level set method is implemented based on a MATLAB toolbox by Sumengen [67]. In this approach, this toolbox is adapted by adding pre-processing steps and the edge based-GACs model. The code is used to process images of size $M \times N$, and pre-processing steps involve contrast stretching and morphological opening and closing. Some images in the databases suffered from poor contrast due to the limited dynamic range of the image sensor during image acquisition, and simple contrast stretching is found to be effective to compensate for this. Morphological opening and closing is used to create an initial estimate the cell

foreground, and to remove narrow links between lobes and cell bulges. A ball structuring element of radius 5 and height 10 is used here. These dimensions are chosen experimentally based on the average size of a cell, and found to work well for the images in the three databases used. After pre-processing, our method based on level set forces via GACs method is applied as summarised in pseudo-code in Algorithm-1.

3.2.1. Parameter Selection

Parameters, such as V_0 and the number of iterations have to be carefully selected in order to optimise the performance of the proposed method, as will be shown later in Section 3.2.2. In this case, all parameters are experimentally chosen.

In the case of *curvature-based forces and GACs*, the parameters are chosen as follows: $\alpha = 0.3$, $V_0 = 0.5$ and number of iterations = 5. This parameter α balances the regularity of the curve and its smoothness with each iteration, and its value is chosen to be greater than 0 so that the interface moves in the normal direction, and the curve becomes smooth and shrinks. In this case, this procedure involves computing the curvature-based force and the GAC until the curve evaluation closely matches the cell boundary of the gradient g of the image. The value of g becomes greater than 0 when the curve approaches the edges, and strong edges stop propagation of the curve. The results are shown in Fig-2.

Algorithm 1 Level Set Forces Via GACs

Require: Level set via GACs

Input: Image $I(x, y)$, positive number of iterations n, forces $\alpha\kappa$, V_n and $\overrightarrow{S}$, and stopping function $g(I(x, y))$

Output: Segmented nuclei of WBCs

1. Calculate zero level set C (see Eq.(1)).
2. Initialize signed distance $\phi(x, y = \pm d((x, y), C)$ (see Eq.(2)).
3. Calculate stopping function $g(I(x, y))$ (see Eq.(11)).
4. **switch** Level set forces **do**

- **case** Curvature-based force via GACs
  - (a) Initialize constants α and V_0
  - (b) Calculate the Euler time step $\triangle t$ (see Eq.(6)).
  - (c) **while** iterations $\leq n$ **do**
    - i. $\phi_{t+1} = \phi_t - (g(I(x, y))(\alpha\kappa + V_0)\,|\nabla\phi(x, y, t)|)\triangle t$ (see Eq.(10))
    - ii. Update time $t = t + \triangle t$
    - iii. iterations = iterations + 1
  - (d) **end while**
- **case** Force in the normal direction via GACs
  - (a) Initialize constants V_n and V_0
  - (b) **while** iterations $\leq n$ **do**
    - i. Calculate the Euler time step $\triangle t$ (see Eq.(6)).
    - ii. $\phi_{t+1} = \phi_t - (g(I(x, y))(V_n + V_0)\,|\nabla\phi(x, y, t)|)\triangle t$ (see Eq.(13))
    - iii. Update time $t = t + \triangle t$
    - iv. iterations = iterations + 1
  - (c) **end while**
- **case** Vector field-based force via GACs
  - (a) Initialize constant V_0
  - (b) Calculate components of vector field u and v (see Eq.(15)).
  - (c) **while** iterations $\leq n$ **do**
    - i. Calculate $\overrightarrow{S}$ using upwind differencing
    - ii. Calculate the Euler time step $\triangle t$ (see Eq.(6)).
    - iii. $\phi_{t+1} = \phi_t - (g(I(x, y))(\overrightarrow{S} + V_0)\,|\nabla\phi(x, y, t)|)\triangle t$ (see Eq.(16))
    - iv. Update time $t = t + \triangle t$
    - v. iterations = iterations + 1
  - (d) **end while**

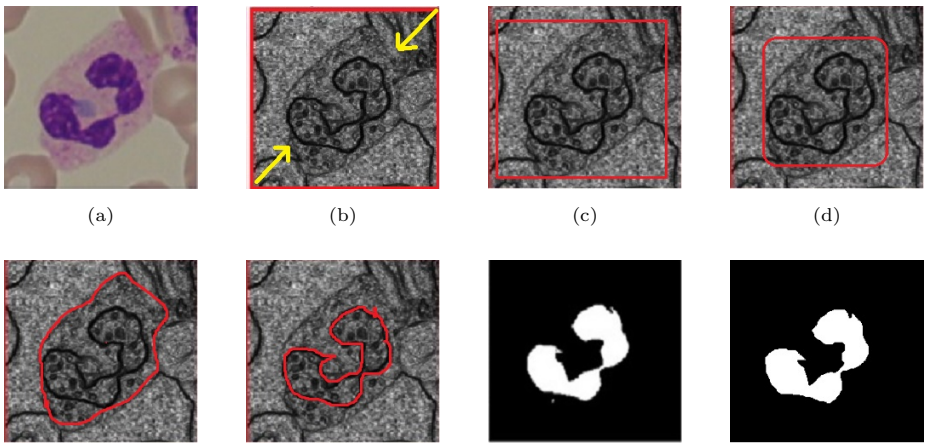

Figure 2: A neutrophil nucleus segmented using the level set method with *curvature-based forces* and GACs. The contour is represented in red and the yellow arrows represent the force V_0. (a) Cell image from [65]; (b) iteration-1; (c) iteration-2; (d) iteration-3; (e) Iteration-4; (f) iteration-5 – showing how the curve (level set) closely matches the cell boundary; (g) detected cell; and (h) ground truth.

The parameters chosen in the case of our proposed the level set method using *forces in the normal direction with GACs* are $V_n = 10$, $V_0 = 100$ and number of *iterations* $= 5$. In this case, the curve representation follows the motion in the normal direction as $(V_n + V_0)|\nabla\phi(x, y, t)|$. The value of V_n should be greater than 0 in order to move outwards in the normal direction. V_0 is the force that pushes the curve in the normal direction of the contour until it converges with the boundary of the gradient g of the image and the weak edges disappear. The results are shown in Fig-3.

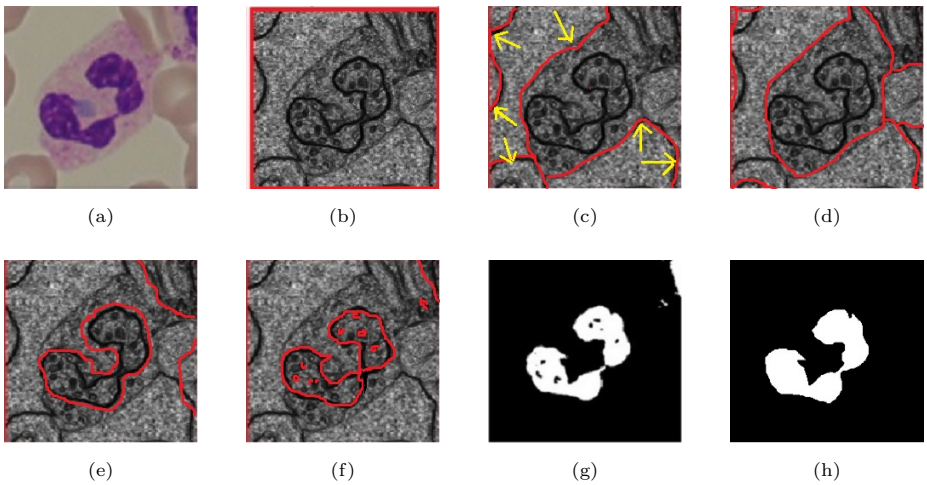

Figure 3: A Neutrophil nucleus segmented using the level set method with *forces in the normal direction* and GACs. The contour is represented in red and the yellow arrows represent the force V_0. (a) Cell image from [65]; (b) iteration-1; (c) iteration-2; (d) iteration-3; (e) iteration-4; (f) iteration-5 – showing how the curve (level set) closely matches the cell boundary; (g) detected cell; and (h) ground truth.

In the case of *vector field-based forces and GACs*, the parameters are chosen as follows: $u = -2.1216$, $v = -2.1216$, $V_0 = 20$ and number of iterations = 5. In this case, the force motion in the vector field direction, $\overrightarrow{S}$, is based on the values of u and v calculated from Equation-15. The values of u and v must be negative in order to shrink the contours. V_0 represents the external force that pushes the contour towards the gradient g of the image until it closely matches the boundary of the nucleus. The results are shown in Fig-4.

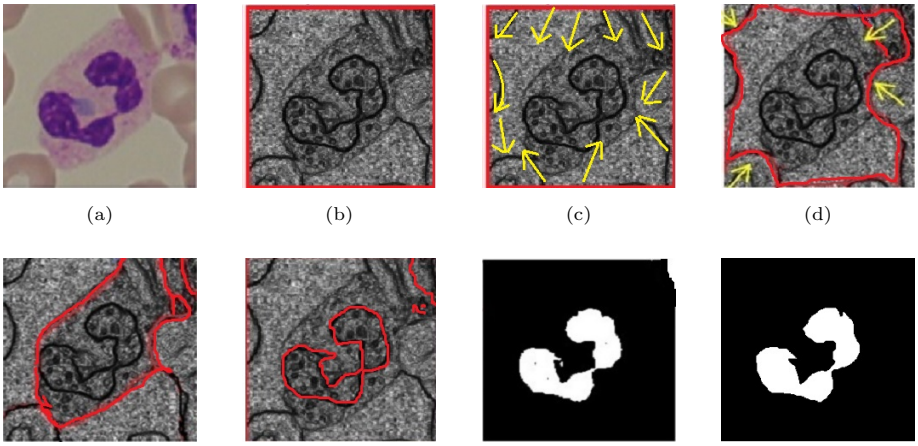

Figure 4: A neutrophil nucleus segmented using the level set method with *vector field-based forces* and GACs. The contour is represented in red and the yellow arrows represent the force V_0. (a) Cell image from [65]; (b) iteration-1; (c) iteration-2; (d) iteration-3; (e) iteration-4; (f) Iteration-5 – showing how the curve (level set) closely matches the cell boundary; (g) detected cell; and (h) ground truth.

3.2.2. Effects of Parameters

The effects of parameter selection are discussed next. As previously mentioned in Section 3.2.1, parameters such as V_0 and the number of iterations have to be carefully selected in order to optimise the performance of the proposed method.

The value of V_0 affects the detection of the cell boundary differently, depending on the force, as discussed next.

- *Curvature-based forces*
  - $V_0 \leq -1$. Here, the cell cannot be detected correctly because the internal force κ becomes greater than the external force V_0. As a result, the cell shape expands and the cell structure is lost, as shown in Fig-5(a).
  - $-1 \geq V_0 \leq 1$. The use of a curvature-based force via GACs retains the concave shape and topology of the WBC nucleus. As shown in Fig-5(b), it preserves the perceptual edge property of the active contours and the concavity.

– $V_0 \geq 1$. V_0 has greater pushing than κ to the cell boundary, so the WBC nucleus cannot be detected, as shown in Fig-5(c).

(a) (b) (c)

Figure 5: A neutrophil nucleus segmented using curvature-based forces and GACs with parameters $\alpha = 0.3$, 5 iterations, and (a) $V_0 = -2.5$; (b) $V_0 = 0.5$; and (c) $V_0 = 5$.

- *Forces in the normal direction*

  – $V_0 \leq 0$. Holes appear in the segmented nucleus, as shown in Fig-6(a), however, the gap between the lobes and perceptual edges are preserved. The holes can be removed by increasing the value of V_n.

  – $0 < V_0 \leq 100$. The algorithm preserves the concavity and edges, although there are holes which need to be considered, as shown in Fig-6(b).

  – $V_0 > 100$. The segmentation is not correct because V_0 is greater than the level set force in the normal direction V_n and continues to push the contour until the lobes split, as shown in Fig-6(c).

(a) (b) (c)

Figure 6: A neutrophil nucleus segmented using level set methods with forces in the normal direction and GACs using $V_n = 10$, 5 iterations, and (a) $V_0 = -2$; (b) $V_0 = 100$; and (c) $V_0 = 150$.

- *Vector field-based force*

  – $V_0 \leq 0$. The shape of the nucleus and the gap between the lobes are preserved. Here, V_0 helps the force $\overrightarrow{S}$ defined by u and v to shrink the contour until it gets to the boundary, however, there is a certain amount of noise and several holes in the image, as shown in Fig-7(a).

  – $0 < V_0 < 100$. Since V_0 is positive, the external force is slightly greater than $\overrightarrow{S}$, meaning that it can correctly push the contour to the boundary of the cell, as shown in Fig-7(b).

– $V_0 \geq 100$. In this case, the external force V_0 is much greater than $\overrightarrow{S}$, meaning that the contour can not meet the cell boundary and the nucleus cannot be detected, as shown in Fig-7(c).

(a) (b) (c)

Figure 7: A neutrophil nucleus segmented using the level set method with vector field-based forces and GACs using $u = -2.1216$, $v = -2.1216$, 5 iterations, and (a) $V_0 = -5$; (b) $V_0 = 20$; and (c) $V_0 = 120$.

The number of iterations may also affect the resulting segmented nuclei. The results are calculated here using number of iterations 5. When the number of iterations increases significantly (e.g. number of iterations = 100, as shown in Fig-8), the level set method via GACs using *curvature-based forces* cannot preserve the edges, as the strong edges disappear. When *forces in the normal direction* are used, the sharp corners are smoothed and there is some noise that needs to be considered. Finally, in the case of *vector field-based forces*, although the edges of the nucleus are sharp and the concave shape is retained, narrow regions are not properly dealt with.

(a) (b) (c)

Figure 8: A neutrophil nucleus segmented using level set forces via GACs with number of iterations = 100. (a) Curvature-based force; (b) force in the normal direction; and (c) vector field-based force.

3.3. Results and Evaluation

3.3.1. Performance of Proposed Method with Three Forces via GACs

The segmentation performance of the proposed framework is evaluated here based on the F-index, which is used to measure the accuracy of segmentation and to compare the segmentation performance results of the three level set forces. This index is computed based on precision P and recall R. P represents the number of correct positive results divided by the total number of positive results while R represents the number of correct positive results divided by the number of positive results that should have been returned. Both P and R are calculated based on the number of true positives TP, which represent the intersection between the segmentation result and the ground

truth (i.e. pixels correctly segmented as foreground), false positives *FP*, which measure the result of the segmented area that is not in the ground truth (i.e.pixels falsely segmented as foreground), false negatives *FN*, which represent missed parts of the ground truth (i.e.pixels falsely detected as background), and true negatives *TN*, which represent the area that does not belong to the union of the segmentation result and the ground truth (i.e. pixels correctly detected as background). The highest possible value of the F-index is 1, which represents the optimum segmentation [68, 69]. The F-index is calculated as follows:

$$P = \frac{TP}{TP + FP} \tag{17}$$

$$R = \frac{TP}{TP + FN} \tag{18}$$

$$F - Index = 2 \cdot \frac{P \cdot R}{P + R} \tag{19}$$

Table 1 shows a comparison between the performance of the proposed segmentation framework for each type and sub-type of WBC. The average values of the F-index are calculated for the proposed segmentation method using the 750 WBC images from the database. It can be seen that, in most cases, the F-index obtained using curvature-based forces is higher and more stable than the value obtained when using the other two forces. The results obtained with forces in the normal direction are only marginally better than those obtained with vector field-based forces.

Table 1: Performance evaluation of the proposed segmentation framework level set forces via GACs using average F-index for WBC types, where Force-1: curvature-based forces, Force-2: forces in the normal direction, and Force-3: vector field-based forces.

(Sub-)type	**No. images**	**F-index Force-1 (curvature-based)**	**F-index Force-2 (normal direction-based)**	**F-index Force-3 (vector field-based)**
Granulocyte	90	0.9280	0.9360	0.9317
Monocyte	100	0.9251	0.9150	0.9006
Lymphocyte	100	0.9290	0.9305	0.9213
Neutrophil	100	0.9273	0.9234	0.9135
Basophils	80	0.9160	0.9006	0.9001
Eosinophil	80	0.9195	0.8903	0.8891
Macrophages	70	0.8912	0.8800	0.8883
Dendritic	40	0.9009	0.8732	0.8753
B-cell	45	0.9129	0.8915	0.9032
T-cell	45	0.9422	0.9327	0.9320
Average F-index	750	0.9209 ± 0.0640	0.9113 ± 0.0723	0.9076 ± 0.0746

Figure-9 to Figure-11 show the performance obtained in terms of the F-index values, which are plotted on the y-axis, and the image number, which is shown on the x-axis. The same database was used in all cases shown in Fig-9 to Figure-11. Images are numbered according to sub-type, as

follows: granulocyte (90 images): 1-90; monocyte (100 images): 91-190; Lymphocyte (100 images): 191-290; neutrophil (100 images): 291-390; basophil (80 images): 391-470; eosinophil (80 images): 470-550; macrophage (70 images): 551-620; dendritic (40 images): 621-660; B-cell (45 images): 661-705; T-cell (45 images): 706-750. As shown in Fig-9 for curvature-based forces, there are four images with an F-index lower than 0.5 (poor segmentation), while the rest have an F-index between 0.7 and 1 (good segmentation). Fig-10 shows the result of forces in the normal direction, where six images have an F-index lower than 0.5 (poor segmentation), and the rest have an F-index between 0.6 and 1 (good segmentation, but not as good as in the case of curvature-based forces in all cases). Finally, Fig-11 shows the results for vector field-based forces. In this case, four images have been poorly segmented (with an F-index lower than 0.5), and the rest are better segmented (with an F-index between 0.5 and 1, which is lower than in the previous two cases).

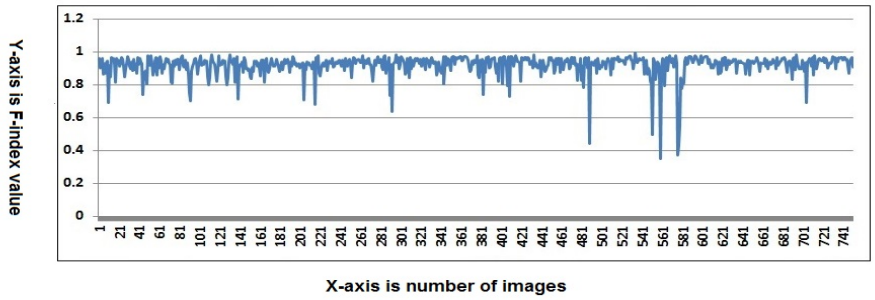

Figure 9: F-index performance values obtained for the level set using *curvature-based forces* and GACs. F-index is value plotted along the y-axis, and the image number is plotted along the x-axis.

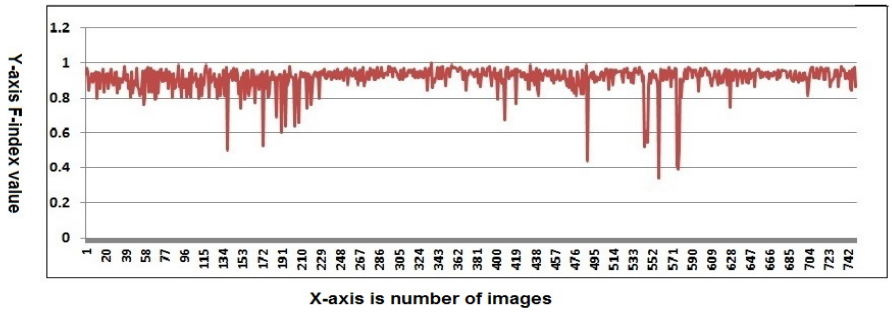

Figure 10: F-index performance values obtained for the level set using *forces in the normal direction* and GACs. F-index value is plotted along the y-axis, and the image number is plotted along the x-axis.

The proposed level set-based forces via edge-based GACs is tested using an Intel(R) Core(TM) i7-4600U CPU 2.70 GHz processor. The proposed method with curvature force via GACs has an average runtime of $0.64s$, while normal direction force via GACs has an average runtime of $0.66s$, and vector field force via GACs has an average runtime of $0.68s$. The results show that our proposed method is significantly faster with the curvature force than with the other forces, which use larger time steps to speed up the curve evolution of the curve while the GACs maintain the

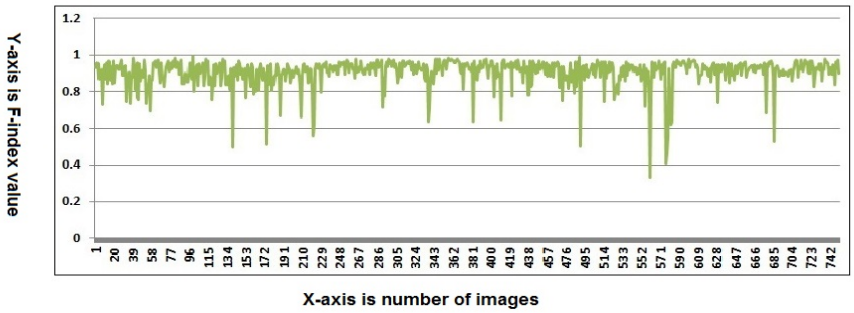

Figure 11: F-index performance values obtained for the level set using *vector field based forces* and GACs. F-index value is plotted along the y-axis, and the image number is plotted along the x-axis.

stable evolution of the level set function.

The performance of the three level set forces, and the results presented in Section 3.3.1, demonstrate that the best segmentation results are obtained for curvature-based forces. In most cases, the F-index obtained using curvature-based forces is higher and more stable than that F-index obtained using the other two forces. The results obtained with forces in the normal direction are only marginally better than those obtained with vector field-based forces. In the case of forces in the normal direction, weak edges are not properly detected when the cell nucleus is undergoing splitting; however, the structure of the cell and concavity are retained. In the case of vector field-based forces, the method behaves better with sharp edges and strong the convexity of the cell.

3.3.2. Comparison and Benchmarking with Other Methods

In this section, average F-index values are computed, for the proposed segmentation method, based on the TP, FP, FN, and TN parameters and are compared with the values of other segmentation methods, including morphological operators [44], edge and boundary detection [5], colour-space-based k-means clustering [7], region detection model and EM [59], fuzzy c-means (FCM) [8], self-supervised learning method [14], dual threshold [9], watershed-based neural network [15], k-means clustering with the watershed algorithm [46], the Chan-Vese method [70] and Otsu's thresholding [10]. As in the previous section, 750 images from the three databases described in Section-3.1 were used to evaluate the performance of all methods. Table-2 shows that the three level set forces via GACs result in better performance than the other methods. The proposed method shows a better ability to detect WBC nuclei than the other 12 methods, which fail to produce good results in cases with complex boundaries, low contrast or where merging and splitting nuclei present. The proposed framework achieves higher accuracy (92.09%, 91.13% and 90.76%) than the best accuracy achieved by the recent methods shown in Table-2, including k-means clustering with the watershed algorithm [46], thresholding and manifold low-rank [12], colour-based k-means clustering [7] and edge and boundary detection [5], although the accuracy the method of the k-means clustering approach [46] is almost equal to that of our proposed method.

Table 2: Performance comparison (average F-index) of the proposed segmentation framework (level set based three forces via GACs) with 12 other methods for WBC nucleus segmentation using the same database (750 images from [64, 65, 66]).

Method name	**TP**	**FP**	**FN**	**TN**	**F-index value**
Morphological operators [44]	466	85	195	4	0.7696 ± 0.05346
Edge and boundary detection [5]	510	87	148	5	0.8108 ± 0.0518
Colour-based k-means clustering [7]	520	85	136	9	0.8246 ± 0.1853
Fuzzy c-means (FCM) [8]	427	105	169	49	0.7571 ± 0.0892
Region detection model and EM [59]	458	130	112	50	0.7910 ± 0.1723
Dual threshold [9]	420	120	170	40	0.7433 ± 0.0522
Chan-Vese method [70]	319	227	180	24	0.6107 ± 0.0705
Otsu's thresholding [10]	240	230	180	100	0.5390 ± 0.2109
Thresholding and manifold low-rank [12]	590	60	100	0	0.8805 ± 0.0226
Clustering and watershed algorithm [46]	620	30	100	0	0.9021 ± 0.0631
Self-supervised learning method [14]	475	100	165	10	0.7816 ± 0.1659
Watershed-based neural network [15]	449	103	185	13	0.7573 ± 0.1779
(Our proposed-1)	649	0	101	0	**0.9209 ± 0.0640**
(Our proposed-2)	628	25	97	0	**0.9113 ± 0.0723**
(Our proposed-3)	623	25	102	0	**0.9076 ± 0.0746**

Table-3 shows a comparison of the performance indices for the proposed segmentation method with the other methods. Average values were computed for the proposed segmentation method using 750 images from three databases [64, 65, 66], and are compared with the average values achieved by the existing methods. To quantify the segmentation results and to evaluate the stability of the proposed segmentation framework, three indices are used: Jaccard distance (JD), boundary displacement error (BDE), and rand index (RI). The performance of the proposed technique is benchmarked against the 12 other algorithms. As can be seen from Table-3, the proposed segmentation method results in better performance than the other techniques for all indices except BDE, where the self-supervised learning method [14] and watershed-based neural network [15] are marginally better.

3.4. Qualitative Results of Proposed Method and Other Methods

Fig-12 shows qualitative results of the performance of the level set method via edge-based GACs for different topology changes of nuclei shapes. As can be observed, curvature forces have the ability

Table 3: Comparison of different WBC segmentation methods using three indices. The proposed segmentation framework (level set-based three forces via GACs) compared with the 12 other methods for WBC nucleus segmentation over the same databases(using 750 images from [64, 65, 66]). The best results are highlighted in bold.

Method name	**JD**	**RI**	**BDE**
Morphological operators [44]	0.3123	0.7541	15.1213
Edge and boundary detection [5]	0.2122	0.7512	14.3421
Colour-based k-means clustering [7]	0.2976	0.7483	15.4301
Fuzzy c-means (FCM) [8]	0.2941	0.7454	15.2341
Region detection model and EM [59]	0.1231	0.7425	16.4512
Dual threshold [9]	0.1954	0.6696	N/A
Chan-Vese method [70]	0.2312	0.7367	N/A
Otsu's thresholding [10]	0.4351	0.7338	14.2341
Thresholding and manifold low-rank [12]	0.0142	0.8909	11.0012
Clustering and watershed algorithm [46]	0.0159	0.8628	12.4234
Self-supervised learning method [14]	0.1023	0.8251	10.3012
Watershed-based neural network [15]	0.0566	0.7902	10.1245
Our proposed force-1 via GACs	**0.0025**	**0.9176**	**10.4561**
Our proposed force-2 via GACs	**0.0035**	**0.9005**	**11.4411**
Our proposed force-3 via GACs	**0.0033**	**0.8902**	**11.2341**

to discriminate the nucleus from the cytoplasm and adjacent erythrocytes, addressing problem of detection of the WBC nucleus detection problem despite the presence of concavity, convexity, sharp corners, merging and splitting lobes.

Fig-13 shows an example in which our proposed method and the others listed above are used to segment a WBC nucleus with concavities, boundary gaps, sharp corners, low contrast, weak edges and merging. As shown in Fig-13 (b,c,d), using the level set forces (curvature, normal direction and vector field) via edge-based GACs results in a single nucleus, which allows us to identify the cell as a neutrophil. Fig-13 (f) shows that FCM segmentation results in three lobes rather than one, meaning that the WBC identified as a different type of WBC. Fig-13 (g) shows that colour-space-based k-means clustering results in two lobes, leading the WBC to be identified as an eosinophil, when in fact it is a neutrophil. The WBC nucleus is not always prominent and straightforward to segment, particularly when thresholding techniques, such as dual threshold [9] and Otsu's thresholding [10] are used, and the results show that thresholding techniques cannot properly address changes in curve topology, such as splitting, merging, convexity, concavity and sharp corners of lobes even when the colour of the WBC nuclei is prominent. Consequently, they cannot detect WBC nuclei correctly,

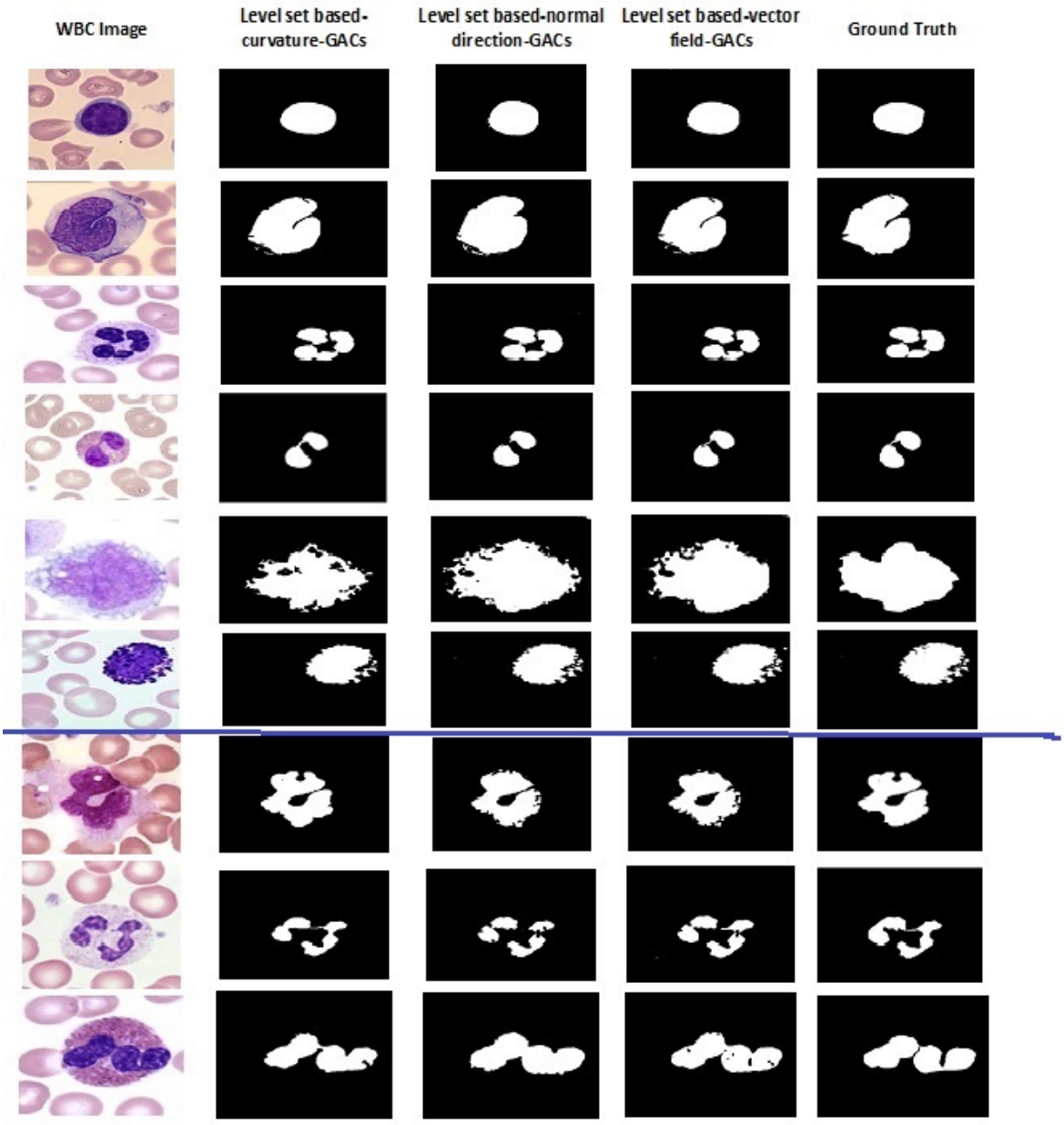

Figure 12: Qualitative results of the level set method via edge-based GACs for simple topology changes of nuclei shapes (above blue line), including merge, split, sharp corners and concavity, and difficult topology changes and complicated nuclei shapes (below blue line). The examples also focus on texture, position, colour distribution, phases of maturation, background, size, deformations, lobes, and staining. Types and sub-types of WBCs from [65, 64, 66] are shown in the first column. Results obtained with the level set method via GACs using different forces are shown in columns two to four. The ground truth is shown in the last column.

as shown in Fig-13 (h) and Fig-13 (e). Fig-13 (e) shows that the dual threshold method cannot deal with convexity and concavity. Fig-13 (h) demonstrates that Otsu's thresholding keeps the gap between the lobes, but a problem persists with concavity and sharp corners, which are considerably

smoothed, and further image preprocessing is needed when using this method to remove undesired information. Finally, Fig-13 (i) shows that the Chan-Vese method cannot detect the shape and location of the nucleus because it uses the intensity between regions rather than edges, as shown by the fact that an erythrocyte is detected instead of the WBC due to its higher contrast. The dual threshold, FCM, colour space-based k-means clustering, Otsu's thresholding and Chan-Vese methods cannot properly address changes in curve topology, and the splitting and merging of lobes; this means that they cannot detect WBC nuclei correctly in contrast to level set-based (curvature, normal direction and vector field) forces via edge-based GACs. The final result shows the ability of our proposed method to obtain more accurate boundaries despite gaps and concavities in the nucleus. This comparison enables us to make a decision based on the results of the evaluation to use the cell segmentation in classification investigation, and obtain benchmarking results. Segmented WBC nuclei have been used in the investigation of feature extraction and classification of WBCs in [16, 17].

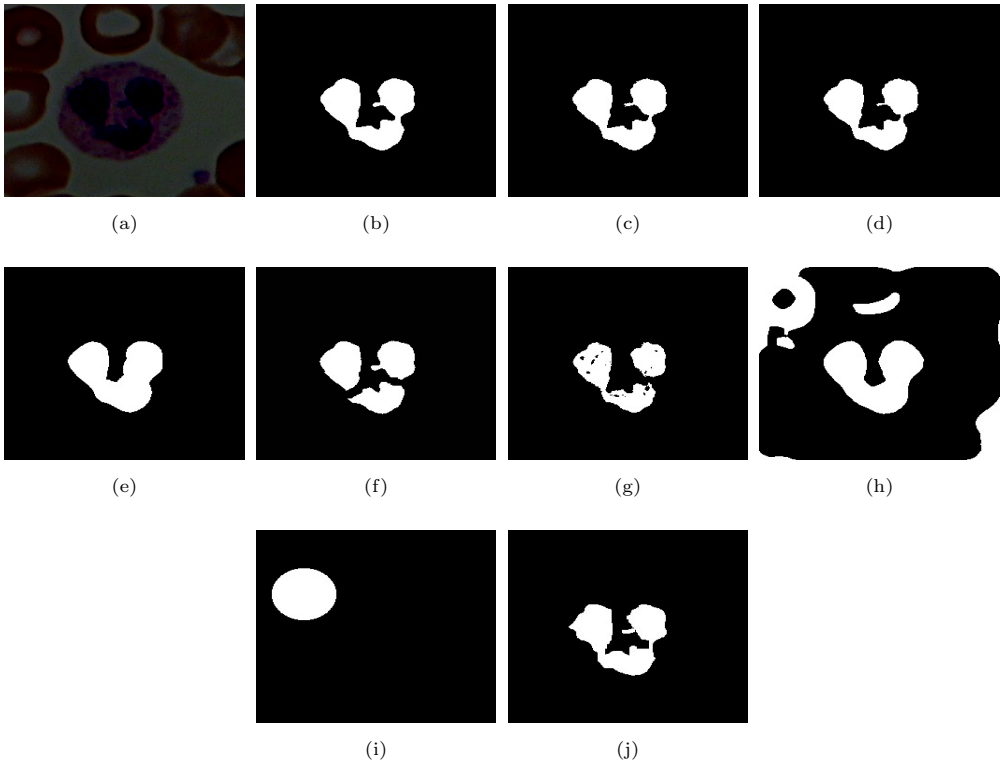

Figure 13: (a) An example of neutrophil nucleus image (weak edge); segmented nucleus using (b) level set with curvature force and GACs; (c) level set with normal direction-based force and GACs; (d) level set with vector field-based forces and GACs; (e) dual threshold method; (f) FCM; (g) colour space-based k-means clustering, (h) Otsu's thresholding; (i) Chan-Vese method; and (j) ground truth.

4. Conclusion

In this paper, we propose a method based on level set method via edge- based GACs using different forces (curvature, normal direction and vector field) for the segmentation of the WBC nucleus. These three level set forces can be used with edge-based GACs to extract the complex shapes of WBC nuclei because they can represent intricate details. The proposed method is demonstrated to be highly versatile depending on the selection of the different parameters. Testing is carried out using 750 WBC images at different stages of maturity and with varying illumination, orientation and background, with no prior knowledge of the target shape. The obtained results are satisfactory, despite the wide variations in the images. The performance of the proposed method has been evaluated using the F-index measure, and the results show that the best segmentation results are obtained for curvature-based forces, with an average F-index equal to $0.921^{\pm 0.064}$. The results obtain with forces in the normal direction are marginally better than those obtain with vector field-based forces. The F-index values obtain with forces in the normal direction and vector field-based forces are $0.911^{\pm 0.072}$ and $0.908^{\pm 0.075}$, respectively. The performance of the proposed framework has also been compared with and benchmarked against 12 other WBC segmentation methods using the same database. The proposed algorithm yields better segmentation results according to the F-index, with values of over 0.9 while the best results from the other methods are: 0.90 for (k-Means clustering with a watershed algorithm), 0.82 for (colour-based k-means clustering), and 0.81 for (edge and boundary detection). Higher performance is obtained using the proposed segmentation method since: (a) level set three forces via edge-based GACs can better handle topological changes, including concavity, convexity, broken edges and merging during the evolution of curves for a reduced number of iterations; (b) the proposed method has the ability to detect the nuclei of WBCs and to obtain reliable information related to the shape of the nucleus for each type of WBC; (c) it works well with strong edges as these stop propagation of the curve and preserve the perceptual edge property of active contours; and (d) it has the capacity to segment different regions with different intensities. In previous work [18], an experiment was conducted on a small number of images containing multiple cells, and the results were superior with a low error rate using the level set method via GACs in this work. The level set-based curvature force method via edge-based GACs was also applied to Hep-2 specimen images containing multiple cells in [71]. In this work, the proposed framework did not consider overlapped cells since it was not been applied to images containing multiple cells. The problems of overlapping cells and cytoplasm segmentation will be considered in future work.

References

[1] Z. Liu, J. Liu, X. Xiao, H. Yuan, X. Li, J. Chang, C. Zheng, Segmentation of white blood cells through nucleus mark watershed operations and mean shift clustering, Sensors 15 (9) (2015)

22561–22586, https://doi.org/10.3390/s150922561.

[2] J. Kemal, Laboratory manual and review on clinical pathology, OMICS Group.

[3] H. Diem, T. Haferlach, H. Theml, Color Atlas of Hematology: Practical Microscopic and Clinical Diagnosis, Thieme, 2004, http://www.chospab.es/biblioteca/DOCUMENTOS/Color_Atlas_of_Hematology_Practical_and_Clinical_Diagnosis_2004_Thieme.pdf.

[4] K. AL-Dulaimi, J. Banks, V. Chandran, I. Tomeo-Reyes, K. Nguyen, Classification of white blood cell types from microscope images: Techniques and challenges, in: Microscopy Science: Last Approaches on Educational Programs and Applied Research, Vol. 8, Formatex Research Center, 2018, pp. 17–25, https://eprints.qut.edu.au/121783/.

[5] F. Sadeghian, Z. Seman, B. H. A. Ramli, Abdul Rahman andKahar, M.-I. Saripan, A framework for white blood cell segmentation in microscopic blood images using digital image processing, Journal of Biological Procedures (online) 11 (1) (2009) 196, http://doi.org/10.1007/s12575-009-9011-2.

[6] L. B. Dorini, R. Minetto, N. J. Leite, Semiautomatic white blood cell segmentation based on multiscale analysis, IEEE Journal of Biomedical and Health Informatics 17 (1) (2013) 250–256, https://doi.org/10.1109/TITB.2012.2207398.

[7] C. Zhang, X. Xiao, X. Li, Y.-J. Chen, W. Zhen, J. Chang, C. Zheng, Z. Liu, White blood cell segmentation by color-space-based k-means clustering, Sensors 14 (9) (2014) 16128–16147, http://doi.org/10.3390/s140916128.

[8] P. K. Mondal, U. K. Prodhan, M. S. Al Mamun, M. A. Rahim, K. K. Hossain, Segmentation of white blood cells using fuzzy c means segmentation algorithm, International Organization and Scientific Research (IOSR) Jornal of Computer Engineering 1 (16) (2014) 1–5, https://doi.org/10.1109/CSITSS.2016.7779438.

[9] Y. Li, R. Zhu, L. Mi, Y. Cao, D. Yao, Segmentation of white blood cell from acute lymphoblastic leukemia images using dual-threshold method, Computational and Mathematical Methods in Medicine 2016, http://dx.doi.org/10.1155/2016/9514707.

[10] N. Salem, N. M. Sobhy, M. El Dosoky, A comparative study of white blood cells segmentation using otsu threshold and watershed transformation, Journal of Biomedical Engineering and Medical Imaging 3 (3) (2016) 15, http://doi.org/10.14738/jbemi.33.2078.

[11] J. P. Gowda, S. P. Kumar, Segmentation of white blood cell using k-means and gram-schmidt orthogonalization, Indian Journal of Science and Technology 10 (6), https://doi.org/10.17485/ijst/2017/v10i6/111353.

[12] F. Cao, M. Cai, J. Chu, J. Zhao, Z. Zhou, A novel segmentation algorithm for nucleus in white blood cells based on low-rank representation, Neural Computing and Applications 28 (1) (2017) 503–511, https://doi.org/10.1007/s00521-016-2391-8.

[13] S. N. M. Safuan, M. R. M. Tomari, W. N. W. Zakaria, White blood cell (wbc) counting analysis in blood smear images using various color segmentation methods, Measurement 116 (2018) 543–555, https://doi.org/10.1016/j.measurement.2017.11.002.

[14] X. Zheng, Y. Wang, G. Wang, J. Liu, Fast and robust segmentation of white blood cell images by self-supervised learning, Micron 107 (2018) 55–71, https://doi.org/10.1016/j.micron.2018.01.010.

[15] H. Miao, C. Xiao, Simultaneous segmentation of leukocyte and erythrocyte in microscopic images using a marker-controlled watershed algorithm, Computational and Mathematical Methods in Medicine 2018, https://doi.org/10.1155/2018/7235795.

[16] K. Al-Dulaimi, K. Nguyen, J. Banks, V. Chandran, I. Tomeo-Reyes, Classification of white blood cells using l-moments invariant features of nuclei shape, in: International Conference on Image and Vision Computing New Zealand (IVCNZ), IEEE, 2018, pp. 1–6, https://doi.org/10.1109/IVCNZ.2018.8634678.

[17] K. AL-Dulaimi, V. Chandran, J. Bank, I. Tomeo-Reyes, K. Nguyen, Classification of white blood cells using bispectral invariant features of nuclei shape, in: International Conference on Digital Image Computing: Techniques and Applications (DICTA), IEEE, 2018, pp. 19–27, http://doi.org/10.1109/DICTA.2018.8615762.

[18] K. AL-Dulaimi, I. Tomeo-Reyes, J. Banks, V. Chandran, White blood cell nuclei segmentation using level set methods and geometric active contours, in: International Conference on Digital Image Computing: Techniques and Applications (DICTA), IEEE, 2016, pp. 1–7, https://doi.org/10.1109/DICTA.2016.7797097.

[19] T.-Y. Lin, P. Goyal, R. Girshick, K. He, P. Dollár, Focal loss for dense object detection, IEEE Transactions on Pattern analysis and Machine Intelligence-Https://doi.org/10.1109/TPAMI.2018.2858826.

[20] X. Bai, H. Zhang, J. Zhou, Vhr object detection based on structural feature extraction and query expansion, IEEE Transactions on Geoscience and Remote Sensing 52 (10) (2014) 6508–6520, https://doi.org/10.1109/TGRS.2013.2296782.

[21] K. A. Al-Dulaimi, A. A. R. Al-Saba'awi, Handprint recognition technique based on image segmentation for recognize, International Journal of Computer Information Systems 2 (6) (2011) 7–12.

[22] K. A. Al-Dulaimi, Using feature extraction for human footprints recognition, International Journal of Computer Applications 64 (3) (2013) 39–44, https://doi.org/10.5120/10617-5339.

[23] M. S. Altaei, K. Abbas, M. Jawad, Speaker recognition based on semantic indexing, Engineering and Technology Journal 29 (5) (2011) 935–947, https://pdfs.semanticscholar.org/d60d/db9968a134163c5e21e1e68817e74a3b46d1.pdf.

[24] S. M. Ali, K. A. AL-Phalahi, Face recognition technique based on eigenfaces method, in: 3rd Scientific Conference of the College of Science-Baghdad University-Iraq, 2009, pp. 781–785.

[25] K. Abbas, Eye recognition technique based on eigeneyes method, in: International Conference on Software and Computer Applications, Vol. 9, IACSIT Press, Singapore, 2011, pp. 212–219.

[26] K. S. Kumar, K. Raja, R. Chhotaray, S. Pattnaik, Coherent steganography using segmentation and dct, in: 2010 IEEE International Conference on Computational Intelligence and Computing Research, IEEE, 2010, pp. 1–6, https://doi.org/10.1109/ICCIC.2010.5705870.

[27] K. A. Al-Phalahi, Data concealment technique in background segmentation of color image based secure data transmission system, Al-Nahrain Journal of Science (ANJS) 14 (2) (2011) 189–198, https://doi.org/10.22401/JNUS.14.2.25.

[28] D. N. Hmood, K. A. Khudhiar, M. S. Altaei, A new steganographic method for embedded image in audio file, International Journal of Computer Science and Security (IJCSS) 6 (2) (2012) 135–141.

[29] K. Abbas, M. Rydh, Satellite image classification and segmentation by using JSEG segmentation algorithm, International Journal of Image, Graphics and Signal Processing 4 (10) (2012) 48–54, https://doi.org/10.5815/ijigsp.2012.10.07.

[30] Ö. Yıldırım, P. Pławiak, R.-S. Tan, U. R. Acharya, Arrhythmia detection using deep convolutional neural network with long duration ecg signals, Computers in Biology and Medicine 102 (2018) 411–420, https://doi.org/10.1016/j.compbiomed.2018.09.009.

[31] P. Khojasteh, L. A. P. Júnior, T. Carvalho, E. Rezende, B. Aliahmad, J. P. Papa, D. K. Kumar, Exudate detection in fundus images using deeply-learnable features, Computers in Biology and Medicine 104 (2019) 62–69, https://doi.org/10.1016/j.compbiomed.2018.10.031.

[32] K. Ishihara, T. Ogawa, M. Haseyama, Helicobacter pylori infection detection from gastric x-ray images based on feature fusion and decision fusion, Computers in Biology and Medicine 84 (2017) 69–78, https://doi.org/10.1016/j.compbiomed.2017.03.007.

[33] E. Karimi, L. Menard, C. Laporte, Fully-automated tongue detection in ultrasound images, Computers in Biology and Medicine 11 (2019) 103335, https://doi.org/10.1016/j.compbiomed.2019.103335.

[34] N. Tomita, Y. Y. Cheung, S. Hassanpour, Deep neural networks for automatic detection of osteoporotic vertebral fractures on ct scans, Computers in Biology and Medicine 98 (2018) 8–15, https://doi.org/10.1016/j.compbiomed.2018.05.011.

[35] Y. Kurata, M. Nishio, A. Kido, K. Fujimoto, M. Yakami, H. Isoda, K. Togashi, Automatic segmentation of the uterus on mri using a convolutional neural network, Computers in Biology and Medicine (2019) 103438Https://doi.org/10.1016/j.compbiomed.2019.103438.

[36] S. Salsabili, A. Mukherjee, E. Ukwatta, A. Chan, S. Bainbridge, D. Grynspan, Automated segmentation of villi in histopathology images of placenta, Computers in Biology and Medicine (2019) 103420Https://doi.org/10.1016/j.compbiomed.2019.103420.

[37] L. Chen, C. Shen, Z. Zhou, G. Maquilan, K. Thomas, M. R. Folkert, K. Albuquerque, J. Wang, Accurate segmenting of cervical tumors in pet imaging based on similarity between adjacent slices, Computers in Biology and Medicine 97 (2018) 30–36, https://doi.org/10.1016/j.compbiomed.2018.04.009.

[38] M. Rossman, M. Adjouadi, M. Ayala, I. Yaylali, An interactive interface for seizure focus localization using spect image analysis, Computers in Biology and Medicine 36 (1) (2006) 70–88, https://doi.org/10.1016/j.compbiomed.2004.09.001.

[39] M. Pekala, N. Joshi, T. A. Liu, N. M. Bressler, D. C. DeBuc, P. Burlina, Deep learning based retinal oct segmentation, Computers in Biology and Medicine 114 (2019) 103445, https://doi.org/10.1016/j.compbiomed.2019.103445.

[40] Q. Huang, X. Bai, Y. Li, L. Jin, X. Li, Optimized graph-based segmentation for ultrasound images, Neurocomputing 129 (2014) 216–224, https://doi.org/10.1016/j.neucom.2013.09.038.

[41] D. C. Cireşan, A. Giusti, L. M. Gambardella, J. Schmidhuber, Deep neural networks segment neuronal membranes in electron microscopy images, in: Proceedings of the 25th International Conference on Neural Information Processing Systems, Vol. 2 of NIPS'12, Curran Associates Inc., 2012, pp. 2843–2851, http://dl.acm.org/citation.cfm?id=2999325.2999452.

[42] Z. Xu, Z. Wu, J. Feng, Cfun: Combining faster r-cnn and u-net network for efficient whole heart segmentation, ArXiv Preprint ArXiv:1812.04914.

[43] I. Cseke, A fast segmentation scheme for white blood cell images, in: 11th International Conference on Pattern Recognition on Image, Speech and Signal Analysis (IAPR), Vol. II, IEEE, 1992, pp. 530–533, https://doi.org/ 10.1109/ICPR.1992.202041.

[44] L. B. Dorini, R. Minetto, N. J. Leite, White blood cell segmentation using morphological operators and scale-space analysis, in: Conference of XX Brazilian Symposium

on Computer Graphics and Image Processing (SIBGRAPI), IEEE, 2007, pp. 294–304, https://doi.org/10.1109/SIBGRAPI.2007.33.

[45] S. N. M. Safuan, R. Tomari, W. N. W. Zakaria, N. Othman, White blood cell counting analysis of blood smear images using various segmentation strategies, in: AIP Conference Proceedings, Vol. 1883, AIP Publishing, 2017, pp. 1–9, https://doi.org/10.1063/1.5002036.

[46] N. Ghane, A. Vard, A. Talebi, P. Nematollahy, Segmentation of white blood cells from microscopic images using a novel combination of k-means clustering and modified watershed algorithm, Journal of Medical Signals and Sensors 7 (2) (2017) 92, `https://www.ncbi.nlm.nih.gov/pubmed/28553582`.

[47] S. Osher, J. A. Sethian, Fronts propagating with curvature-dependent speed: algorithms based on hamilton-jacobi formulations, Journal of Computational Physics 79 (1) (1988) 12–49, http://dx.doi.org/10.1016/0021-9991(88)90002-2.

[48] S. Osher, R. Fedkiw, Level set methods and dynamic implicit surfaces, Vol. 153, Springer Science and Business Media, 2006.

[49] C. Xu, A. Yezzi, J. L. Prince, A summary of geometric level-set analogues for a general class of parametric active contour and surface models, in: Proceedings IEEE Workshop on Variational and Level Set Methods in Computer Vision, IEEE, 2001, pp. 104–111, http://doi.org/10.1109/VLSM.2001.938888.

[50] C. Xu, A. Yezzi, J. L. Prince, On the relationship between parametric and geometric active contours, in: Conference Record of the Thirty-Fourth Asilomar on Signals, Systems and Computers, Vol. 1, IEEE, 2000, pp. 483–489, http://doi.org/10.1109/ACSSC.2000.911003.

[51] V. Caselles, F. Catté, T. Coll, F. Dibos, A geometric model for active contours in image processing, Numerische Mathematik 66 (1) (1993) 1–31, https://doi.org/ 10.1007/BF01385685.

[52] N. H. Salman, Level set methods implementation for image levelsets and image contour, International Journal of Computer Science and Network Security (IJCSNS) 9 (11) (2009) 199–202, `http://paper.ijcsns.org/07_book/200911/20091128.pdf`.

[53] S. Ali, A. Madabhushi, An integrated region, boundary, shape-based active contour for multiple object overlap resolution in histological imagery, IEEE Transactions on Medical Imaging 31 (7) (2012) 1448–1460, https://doi.org/10.1109/TMI.2012.2190089.

[54] P. Mesejo, S. Cagnoni, A. Costalunga, D. Valeriani, Segmentation of histological images using a metaheuristic-based level set approach, in: 15th Genetic and Evolutionary Computation Conference Companion (GECCO'13), 2013, pp. 1455–1462, http://doi.org/10.1145/2464576.2466808.

[55] J. Wang, S. Zhao, Z. Liu, Y. Tian, F. Duan, Y. Pan, An active contour model based on adaptive threshold for extraction of cerebral vascular structures, Computational and Mathematical Methods in Medicine 2016, http://dx.doi.org/10.1155/2016/6472397.

[56] X. Deng, T. Lan, Z. Chen, M. Zhang, Q. Tao, Z. Lu, Self-adaptive weighted level set evolution based on local intensity difference for parotid ducts segmentation, Computers in Biology and Medicine 114 (2019) 103432, https://doi.org/10.1016/j.compbiomed.2019.103432.

[57] D. P. Mukherjee, N. Ray, S. T. Acton, Level set analysis for leukocyte detection and tracking, IEEE Transactions on Image Processing 13 (4) (2004) 562–572, https://doi.org/10.1109/TIP.2003.819858.

[58] S. Eom, S. Kim, V. Shin, B. Ahn, Leukocyte segmentation in blood smear images using region-based active contours, in: International Conference on Advanced Concepts for Intelligent Vision Systems, Springer, 2006, pp. 867–876, https://doi.org/10.1007/11864349_79.

[59] C. Kalaiselvi, R. Asokan, R. Priyanka, Robust segmentation of cancer affected white blood cells using modified level set algorithm, International Journal of Simulation: Systems, Science and Technology 14 (9), https://doi.org/10.5013/IJSSST.a.14.01.02.

[60] K. AL-Dulaimi, J. Banks, I. Tomeo-Reyes, V. Chandran, Automatic segmentation of HEp-2 cell fluorescence microscope images using level set method via geometric active contours, in: 23rd International Conference on Pattern Recognition (ICPR), IEEE, 2016, pp. 81–83, https://doi.org/10.1109/ICPR.2016.7899612.

[61] T. A. Ngo, Z. Lu, G. Carneiro, Combining deep learning and level set for the automated segmentation of the left ventricle of the heart from cardiac cine magnetic resonance, Medical Image Analysis 35 (2017) 159–171, https://doi.org/10.1016/j.media.2016.05.009.

[62] M. Airouche, L. Bentabet, M. Zelmat, Image segmentation using active contour model and level set method applied to detect oil spills, in: Proceedings of the World Congress on Engineering, Vol. 1, Lecture Notes in Engineering and Computer Science, 2009, pp. 1–3.

[63] S. Osher, N. Paragios, Geometric level set methods in imaging, vision, and graphics, Springer Science & Business Media, 2003.

[64] Cellavision-Database, Cellavision – leading the way in digital cell morphology, `http://www.cellavision.com/` (2011).

[65] ALL-IDB, Acute lymphoblastic leukemia image database for image processing, `http://crema.di.unimi.it/fscotti/all/` (2005).

[66] Wadsworth-Center, White blood cell images, `http://www.wadsworth.org` (2007).

[67] B. Sumengen, A matlab toolbox implementing level set methods, Vision Research Lab. UC Santa Barbara. Available: http://barissumengen.com/level_set_methods.

[68] C. Gonzalez Rafael, E. Woods Richard, L. Eddins Steven, Digital image processing using matlab, Editorial Pearson-Prentice Hall. USA.

[69] C. M. Bishop, Pattern recognition and machine learning, Vol. 128, Springer Science & Business Media, 2006, `https://oops.uclv.edu.cu/`.

[70] T. F. Chan, L. A. Vese, Active contours without edges, IEEE Transactions on Image Processing 10 (2) (2001) 266–277, https://doi.org/10.1109/83.902291.

[71] K. Al-Dulaimi, V. Chandran, K. Nguyen, J. Banks, I. Tomeo-Reyes, Benchmarking HEp-2 specimen cells classification using linear discriminant analysis on higher order spectra features of cell shape, Pattern Recognition Letters 125 (2019) 534–541, https://doi.org/10.1016/j.patrec.2019.06.020.